Accepted Manuscript

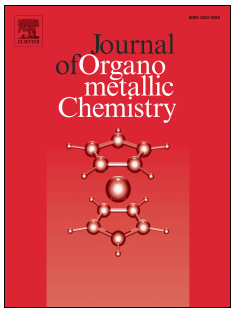

Synthesis and photophysical properties of *ferrocene*-oligo(benzoateethynylene)-fulleropyrrolidines dyads and triads. Implications in photovoltaic cells

J.R. Flores, F. Perez, R.M. Jimenez-Barrera, E. Arias, I. Moggio, R. Torres, G. Rodríguez, M. Ottonelli, R.F. Ziolo

PII: S0022-328X(18)30139-6

DOI: 10.1016/j.jorganchem.2018.02.040

Reference: JOM 20339

To appear in: *Journal of Organometallic Chemistry*

Received Date: 21 November 2017

Revised Date: 21 February 2018

Accepted Date: 23 February 2018

Please cite this article as:

Synthesis and Photophysical Properties of *Ferrocene*- oligo(benzoateethynylene)-fulleropyrrolidines Dyads and Triads. Implications in Photovoltaic Cells

J.R. Flores[1], F. Perez[1], R. M. Jimenez-Barrera[1], E. Arias*[1], I. Moggio*[1], R. Torres[1], G. Rodríguez[1], M. Ottonelli[2], R. F. Ziolo[1]

[1]Centro de Investigación en Química Aplicada, Boulevard Enrique Reyna 140, 25253 Saltillo, Coahuila, México. Tel: +52 844 438 9830, eduardo.arias@ciqa.edu.mx, ivana.moggio@ciqa.edu.mx

[2]Dipartimento di Chimica e Chimica Industriale, Università degli Studi di Genova, Via Dodecaneso 31 I-16146, Genova, Italia

Abstract

A series of fulleropyrrolidines-conjugated bridge-ferrocene or triazene oligomers were selectively synthesized by the Sonogashira reaction by applying the step-by-step approach. The bridge is constituted by 1, 2 and 3 benzoateethynylene units (BzE) and bears triazene (Et_2N_3) or ferrocene as terminal groups affording the **C60-2PEN$_3$** and **C60-3PEN$_3$** dyads and **C60-1PEFe**, **C60-2PEFe** and **C60-3PEFe** triads. DQF-COSY, HETCOR, ^{1}H and ^{13}C NMR and the MALDI-TOF characterization clearly confirmed the expected molecular structure. The absorption spectra of the fulleropyrrolidine oligomers do not match the sum of the individual spectra: N-methylfulleropyrrolidine (NMF) and BzEs, suggesting electronic interaction between the two moieties in the ground state. The fluorescence of the BzE is strongly quenched after functionalization with NMF, which could be indicative of energy or electron transfer from the triazene or ferrocene as electron donor to the fulleropyrrolidine electron acceptor through the π-bridge. The latter process was confirmed by cyclic voltammetry. The strength of the electron-accepting group gets to increase anodically the oxidation potential, or decrease cathodically the reduction potential in the order C60-pyrrolidine>benzoate. The character of the HOMO in the series is defined by the electron-donating ferrocene or triazene moiety, whereas the character of the LUMO is mainly determined by the electron-accepting group and is further supported by theoretical calculations. Photovoltaic devices presented low efficiencies, due to the absorption range of the oligomers being out of the maximum solar irradiance and the inhomogeneous organization in the films.

Keywords: Ferrocene, energy transfer, fullerenes, HOMO-LUMO levels

1. Introduction

Organic photovoltaic technology (OPV) has emerged since the discovery that

photoinduced electron transfer process could be achieved from fullerene as an electron acceptor to conjugated polymers as electron donor materials [1]. The main advantages of OPVs were highlighted in the earliest reports and included the possibility to chemically modulate the energy levels of the active materials to get an efficient photoinduced mechanism, and to process larger individual cells and on any substrate geometry through low cost techniques. Encouraged by these expected advantages, many groups around the world have been searching for both, the most efficient photovoltaic macromolecule and the optimal device configuration. Despite that, and though great improvements have been made in both lines, typical efficiencies for OPV cells are only around 8-10 % in single junction and with a recent breakthrough of 12.7% in a tandem multichromophoric two-subunit configuration [2]. Generally, the photoinduced process is obtained in a so-called heterojunction configuration, where the electron donor (D) and acceptor (A) materials are physically mixed as the active layer. This strategy is usually more practical as it opens the way to chemically synthesize different D and A materials in order to modulate the optical and electrical properties [3]. However, the photovoltaic performance of the cell is strongly morphology dependent. An interesting approach is the “molecular cable” or “push-pull” system, where D and A are covalently linked units (usually through a π-transport bridge). Although this strategy implies, in general, larger and more complex synthetic work, it is expected to reduce the problems related to the phase segregation and morphology as D/A are chemically bonded. Moreover, as the feasibility of obtaining a photoinduced process can be estimated through the Weller equation [4], the molecular cable materials represent ideal models for understanding the photophysics of organic photovoltaic devices. Among the organic A materials, even though graphene [5], carbon nanotubes [6], and perylenes [7] have been proposed, fullerenes are still the most used [8]. In the literature, a large number of scientific reports on the synthesis of fullerene-oligo(phenylenevinylene)s molecular cable materials (dyads [9], triads [10,11] and more complex systems [12] can be found).

The state of art of fullerene-phenylenethynylene (PE) derivatives, however, is more restricted [13], likely due to the fact that the rigidity of PEs promotes time dependent aggregation, and in agreement with Martin et al. [13b] phenyleneethynylenes present

(PPE) polarization of the triple bonds, their shorter bonds lengths relative molecules with double bonds make that the electron transfer pathway through the PPE bridges is interrupted by the ethynylene bridge, influencing the charge-separation process and explaining the difference in electron-transfer properties between PPEs and PPVs, but the photovoltaic properties of PPEs materials is relatively new.

In this work, we report on the synthesis of a series of oligomers as precursors and models of the oligo(fulleropyrrolidines) with the aim to provide new push pull models for studying intrinsic photovoltaic process in organic materials. The series provides molecules of increasing length where the ferrocene or triazene as the electron-donor group connects to C60-pyrrolidine as the electron-accepting group in a configuration D→π→A. The photophysical study reveals for the two **C60-2PEN$_3$** and **C60-3PEN$_3$** named as dyads and the three **C60-1PEFe**, **C60-2PEFe** and **C60-3PEFe** named as triads, an exergonic photoinduced electron transfer from the ferrocene or triazene to C60-pyrrolidine, upon excitation of either the BzE unit (likely preceded by energy transfer) or the fullerene. This process is also confirmed by cyclic voltammetry, where the electron transfer is achieved from the iron centre of the ferrocene to the electron-accepting group through the π-bridge. The strength of the electron-accepting group gets to increase anodically the oxidation potential, or decrease cathodically the reduction potential. Despite that, at least in solution, the photoinduced process falls in the inverted Marcus region, i.e., charge recombination is expected to occur, which could explain the low efficiencies (η) found in “molecular cable” solar cells. Improvements in η are obtained by using these materials as electron acceptors in substitution of PC60BM in heterojunction solar cells based on poly(3-hexyltiophene) (P3HT). This result suggests that the new materials do not have a balance in the charges, likely because the BzE unit acts not only as a transport bridge but also as electron withdrawing material because of the ester group. In this context, it is however important to mention that the solar cells were fabricated and studied at ambient conditions and under AM1.5 solar simulator irradiation. Higher efficiencies are expected if devices are prepared and analysed in controlled atmosphere and upon selective irradiation (with a UV laser) as reported in other works on cable materials. This work opens the way to design polar C60-PE molecular cable materials with BzE units substituted with, for instance, glycol lateral

chains that could be deposited on active layers from polar solvents e.g. P3HT, PTB7 to form multilayer tandem photovoltaic devices.

2. Results and discussion

2.1 Syntheses and chemical characterization. Prior to the oligomer synthesis, a bifunctional monomer **4** was prepared in three steps, scheme 1. Esterification of **1** was carried out with (9-bromononyloxy)(*tert*-butyl)dimethylsilane by using DBU in toluene at reflux to give **2,** which was Pd cross-coupled with TMSA to obtain **3** in 91 % yield. Desilylation of **3** with $^{-}F^{+}NBu_4$ in THF affords the desired monomer **4** in 90 % yields.

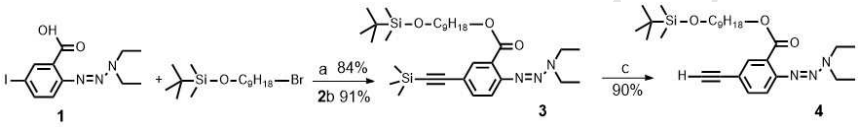

Scheme 1. Reagents and conditions: (**a**) DBU, toluene, reflux, 16h; (**b**) $[(C_6H_5)_3P]_2PdCl_2$ (3.0 % mol), CuI (1.5 % mol), TMSA, Et_3N, 60°C, 16h; (**c**) $^{-}F^{+}NBu_4$, THF, 0°C, 30 min.

The pathway to synthesize the aldehyde-terminated oligomers is described in scheme 2. The convergent-divergent synthesis in general involves three repetitive reactions at each cycle: Sonogashira Pd/Cu cross coupling reaction, iodination and reduction of the aldehyde group.

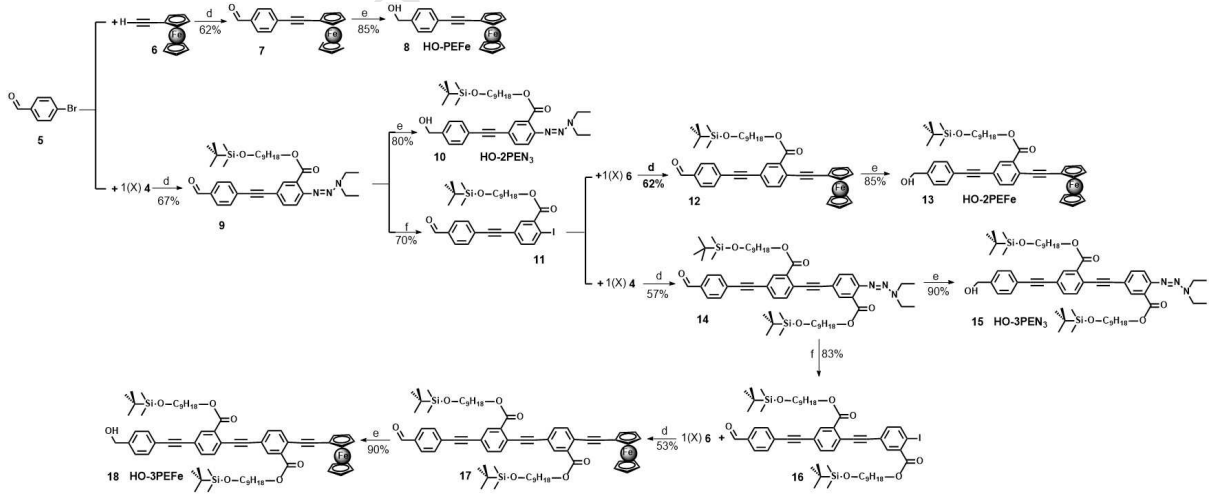

Scheme 2. Reagents and conditions: (**d**) $[(C_6H_5)_3P]_2PdCl_2$ (3.0 % mol), CuI (1.5 % mol), 60°C, 16h; (**e**) $NaBH_4$, THF, N_2, 50°C, 2h; (**f**) CH_3I, 120°C vacuum, 15h.

The oligomerization begins with the Pd/Cu cross coupling of 4-bromobenzaldehyde **5** with commercial ethynylferrocene **6** to generate **7,** which one part is used for the C_{60} cycloaddition and the other part is subjected to the sodium borohydride reduction to obtain the benzyl-alcohol **8**, **HO-PEFe**. It was found that 4 eq. of $NaBH_4$ assure the aldehyde reduction in almost 85-90% yield, however yields also depend on both of the next actions: bubbling the solution with nitrogen before the reaction and not allowing the temperature to pass 60 °C. By Pd/Cu cross-coupling **5** with **4**, the aldehyde-triazene terminated oligomer **9** is obtained. At this point **9** is divided into two portions; one is subjected to the $NaBH_4$ reduction to generate the ethyl alcohol **10**, **HO-2PEN$_3$**, while with the other portion, the triazene is converted to iodine group with iodomethane in a sealed capsule under vacuum. For this reaction, we found that the yield to obtain **11** depends on the precise temperature control at 120°C ± 5°C and on the vigorous stirring of the reaction medium. Then **11** is divided into two portions; one undergoes Pd/Cu cross-coupling with ethynylferrocene to generate **12** (which in turn, one part is used for the C_{60} cycloaddition), while the other part is subjected to the $NaBH_4$ reduction to obtain the ethyl-alcohol **13**, **HO-2PEFe**. The second portion of **11** is subjected to another divergent cycle, by carrying out a Pd/Cu cross-coupling reaction with **4,** affording the aldehyde-triazene terminated oligomer **14**, in which one part is used for the C_{60} cycloaddition and the other for the $NaBH_4$ reduction, generating the ethyl alcohol **15**, **HO-3PEN$_3$**. The triazene conversion of **14** to iodine group in **16** allows its subsequent Pd/Cu cross coupling with ethynylferrocene, forming the aldehyde-ferrocene terminated oligomer **17**; which in turn, one portion is used for the C60 cycloaddition, while the other is subjected to the $NaBH_4$ reduction reaction generating the ethyl alcohol **18**, **HO-3PEFe**. As can be seen, following these repetitive reactions cycles, oligomers can be grown, until they reach the limit of their solubility.

The synthesis route of the fullerene derivatives by the Prato's [14] reaction is depicted in scheme 3. The [3+2] 1,3-dipolar cycloaddition of azomethine ylides generated from the aldehydes **7**, **9**, **12**, **14**, **17** with the sarcosine to the C_{60} gave, in general, yields ranging from 35 to 52 %, as reported in literature [14]. It is worth mentioning that the byproducts

from the reaction consisted of the precursor oligomers but without the aldehyde group. Two series of C_{60}-PEs were synthesized by varying both the oligomer length and the type of termini group: those bearing triazene as terminal group, dyads: **C60-2PEN$_3$** and **C60-3PEN$_3$** and those bearing the ferrocene, tryads: **C60-1PEFe**, **C60-2PEFe** and **C60-3PEFe**. All of the fullerene derivatives are soluble in CH_2Cl_2, $CHCl_3$, toluene, THF and are insoluble in methanol, acetone and acetonitrile. In our original idea, the OH of the 9-nonecanol benzoate side chains was intended to serve as a hydrophilic group that could allow the Langmuir-Blodgett films formation; however, at the moment of cleavage of the *tert*-butyldimethylsilane of the -OH protecting group, the derivative **C60-3PEFe** became insoluble overtime. In addition, we observed that all of the ferrocene compounds with and without fulleropyrrolidines *in solution* are prone to oxidize overtime, likely because ferrocene is not only a good electron donor but an excellent light trapping group that may promote oxidation (*vide infra*). The oxidation process is evidenced because: i) insoluble aggregates are observed, and ii) their ^{1}H NMR spectra develop paramagnetic broad resonant bands instead of the well resolved resonant signals, see Fig 1Sa as example. However, by passing the solution through a plug of alumina, molecules recover their original well-resolved resonant signals, but with at least a 5 % loss of material with each pass. The TGA revealed that fulleropyrrolidines are stable up to 200°C, Fig 1Sb.

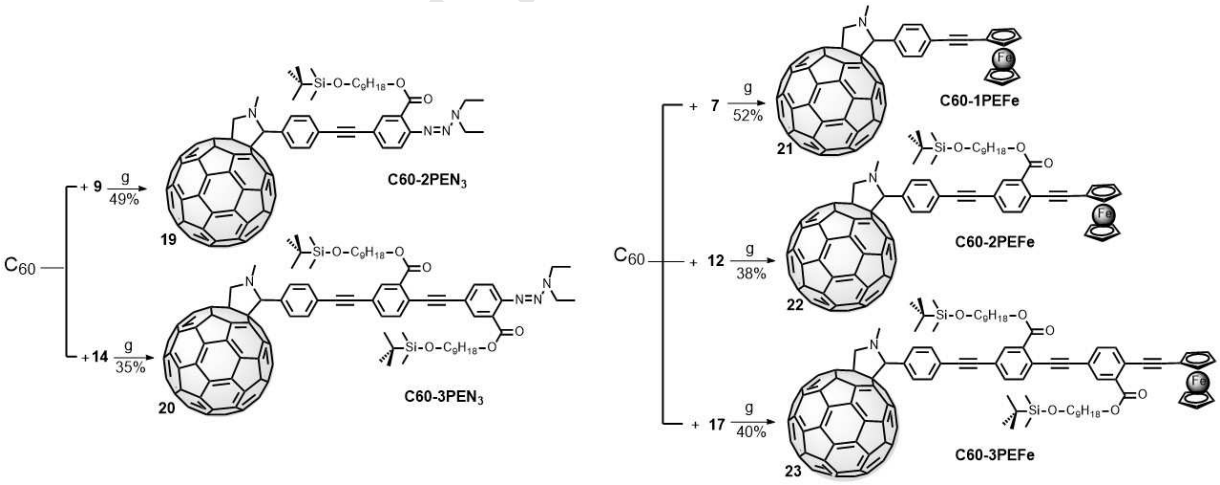

Scheme 3. Reagents and conditions: (**g**) aldehyde (1 eq), C_{60} (1 eq), sarcosine (2.63 eq), toluene (75 mL/100 mg of aldehyde) at reflux, 18h.

The cycloaddition reaction of aldehydes **7**, **9**, **12**, **14** and **17** to the C_{60} is confirmed

because the singlet signal of the aldehydes (~10 ppm) disappears, Fig 4S-5S (ESI) giving rise to the resonance of the pyrrolidine protons, such as that of the $–NCH_3$ group, which clearly appears at 2.8 ppm. As an example of the series, the spectrum of **C60-3PEFe** compound is shown in Figure 1, and the rest of the oligo(fulleropyrrolidines) are shown in Fig 7S. The singlet of the C(2)H-pyrrolidine is centered at 4.95 ppm, while one of the germinal C(1)H1 protons appears as a doublet at 4.96 ppm with a $^3J_{H1\text{-}H2}$ = 9.6 Hz, the other C(1)H2 proton resonates in a high signal density region and is not seen.

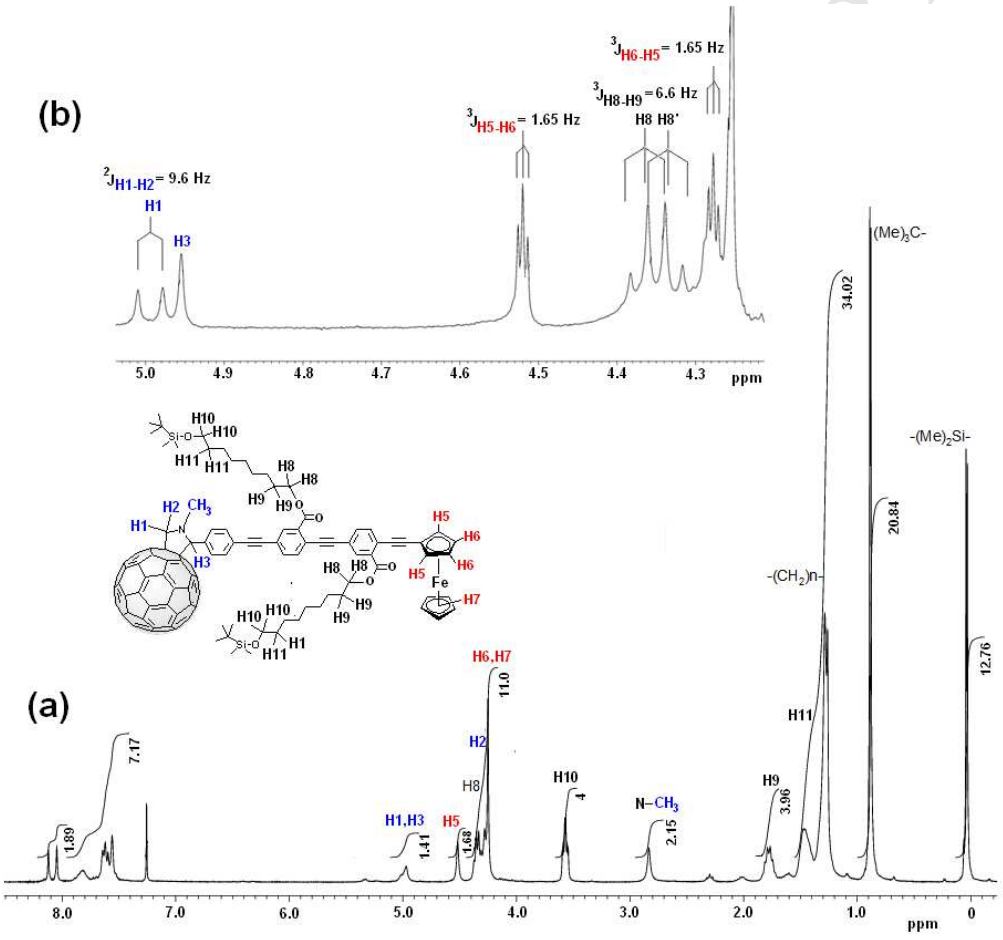

Figure 1. Comparative ^{1}H NMR spectra of **C60-3PEFe** in $CDCl_3$ + CS_2 recorded in: (a) a 300 MHz equipment and (b) in a 500 MHz equipment; multiplicity of H1 and H3 protons are better resolved in a 500 MHz equipment.

In this respect, in the expanded Figure 1b, one can identify those signals of the monosubstituted ferrocene that appear as two triplets at 4.52 ppm (H5,5') and at 4.28 ppm (H6,6') due to their magnetic nonequivalence (giving the interaction of four nuclei

AA'BB' system) with a typical constant $^{3}J_{H5\text{-}H6}$ of 1.65 Hz. Moreover, it is possible to distinguish the quasi-overlapping triplet at 4.34 ppm ($^{3}J_{H8\text{-}H9}$ = 6.6 Hz) that corresponds to the non-chemically equivalents $COOCH_2$ and the singlet at 4.26 ppm of the Cp(H7). The distinctive C(1)H2 proton could be unambiguously assigned by both, DQF and COSY, where the correlation C(1)H1-H2 is clear; as reference, the -N-CH_3 does not correlate with any proton, Fig 8S, and by HETCOR, Fig 9S, where C2 correlates with H3, and C1 with H1 and H2. In what concerns the ^{13}C spectra (broadband decoupling), Fig 10S, the unambiguous chemical shift assignment was achieved by a combination of APT, DEPT-135 ^{13}C, experiments. The lack of C2 or Cs symmetry of the oligo(fulleropyrrolidines) is helpful to differentiate for instance, the two carbonyls that resonate at different displacement, i.e., at 165.85 ppm for C36 and 165.51 for C29. It was also possible to differentiate the 6 ethynylene carbons e.g. for **C60-3PEFe** at 96.40, 95.15, 92.17, 90.5, 88.95, 84.77 ppm. Notice that C2 of the pyrrolidine resonates in the region of the C≡C carbons at 83.34 ppm, while that of the C1 at 70.17 ppm overlaps with those of the Cp(H7). In general, all of the ^{1}H and ^{13}C resonant signals of the fulleropyrrolidines coincide with those reported in literature [15].

All of the **C60-nPEN$_3$** and **C$_{60}$-nPEFe** series were also analyzed by MALDI-TOF mass spectrometry, by using the α-cyano-4-hydroxy cinnamic acid (CHCA) and 2-[(2E)-3-(4-tert-butylphenyl)-2-methylprop-2-enylidene] malonitrile (DCTB) matrices. The molecular ions for all the oligo(fulleropyrrolidines) could be clearly observed with DCTB matrix in the negative ion mode, while in the positive ion mode or with the CHCA matrix, the molecular ion peaks were found to be very weak. For **C60-2PEN$_3$**: *m/z* 1353.55 ($M^{\cdot -}$, calcd for $C_{97}H_{56}N_4O_3Si$: 1352.41); **C60-3PEN$_3$**: *m/z* 1753.80 ($M^{\cdot -}$, calcd for $C_{121}H_{92}N_4O_6Si_2$: 1752.66); **C60-2PEFe**: *m/z* 1461.32 ($M^{\cdot -}$ calcd for $C_{105}H_{55}FeNO_3Si$: 1461.33); **C60-3PEFe**: *m/z* 1861.55 ($M^{\cdot -}$ calcd for $C_{129}H_{91}FeNO_6Si_2$: 1861.57).

2.2 Electrochemical properties

We used cyclic voltammetry to evaluate the donor-acceptor electronic influence of the compounds herein synthesized. The electrochemical data are summarized in Table 1. We observed an insoluble precipitate at the end of the redox analyses in CH_2Cl_2, which confirmed NMR observations of the compounds paramagnetic behaviour once oxidized

[16]. Structurally, the oligomers have a ferrocene, a phenyleneethynylene(s) moiety, a benzoate(s) and or triazene as possible redox groups, while the fulleropyrrolidines in addition have the fullerene-pyrrolidine; both systems are composed of D-(π)bridge-A configuration.

Table 1. Electrochemical properties at the maxima redox potentials of model oligomers and oligo(fulleropyrrolidines) synthetized and studied in this work (0.5 mmol) in CH_2Cl_2, 0.1 M Bu_4NPF as electrolyte, at scan rate of 50 mVs^{-1} (V vs Ag/AgCl) and using GCE as working electrode.

Molecule	E_{red}^{III} (V)	E_{red}^{II} (V)	E_{red}^{I} (V)	E_{ox}^{I} (V)	E_{ox}^{II} (V)	E_{ox}^{III} (V)	HOMO (eV)	LUMO (eV)	Eg (eV)
MFP	−1.523	−1.020	-0.660	+1.386	+2.329		-6.18	-4.14	2.04
Ferrocene			+0.391	+0.482					
HO-2PEN$_3$			-0.970	+1.144	+1.967	+2.433	-5.94	-2.83	3.10
C60-2PEN$_3$		-1.065	-0.868	+1.166	+1.996	+2.430	-5.96	-3.93	2.03
HO-3PEN$_3$		-1.165	-0.860	+0.950	+1.983	+2.350	-5.75	-3.94	1.81
C60-3PEN$_3$		-1.048	-0.828	+1.128	+1.980	+2.300	-5.92	-3.97	1.95
HO-1PEFe			-1.390	+0.816		+1.829	-5.61	-3.41	2.20
C60-1PEFe			-1.220	+0.868		+1.681	-5.66	-3.58	2.09
HO-2PEFe		−1.682	-1.271	+0.609	+0.884	+1.697	-5.40	-3.52	1.88
C60-2PEFe			-1.081	+0.635	+0.903	+1.644	-5.43	-3.72	1.71
HO-3PEFe			-1.025	+0.546	+0.829	+1.613	-5.34	-3.77	1.57
C60-3PEFe			-0.962	+0.575	+0.866	+1.640	-5.37	-3.84	1.54

As a term of comparison, Figure 2 shows the voltammograms of some representative oligomers. In general, we observe in the anodic region, waves originated by the ferrocene, the ester that is overlapped with that of C60 and of the phenyleneethylene groups, while in the cathodic region, just one or maximum two waves were seen. As reference for our study, the calculated ferrocene potentials were of E_{ox} = 0.480 V and E_{red} = 0.391 V (formal potential $E°$ = 0.436 V). The first oxidation potential is thus assigned to the ferrocene, which shifts to higher potentials with respect to the shortest of the oligomer **HO-1PEFe** (0.816 V)**,** however by increasing the conjugation to **HO-**

2PEFe (0.609 V) and to **HO-3PEFe** (0.546 V) a decrease in the oxidation potential is observed, but still with higher values with respect to the free ferrocene. The same trend is observed in the triazene series, but triazene shows to be more difficult to be oxidized and reduced, than ferrocene. The ferrocene oligomers behaviour provides evidence that there is an electron transfer between the iron centre of the ferrocene and the electron-accepting benzoate(s) group and, that in general, phenyleneethynylene's are also difficult to be oxidized (~1.3 V) or reduced (~2.5 V) [17].

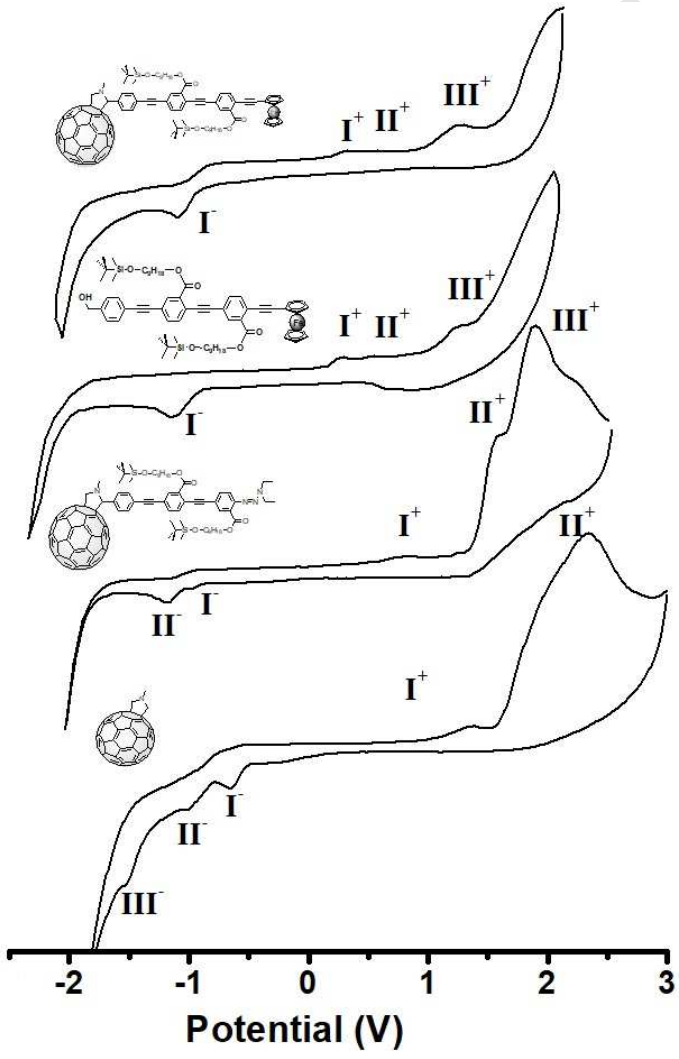

Figure 2. Comparative voltammograms of **MFP**, **C60-3PEN$_3$, HO-3PEFe** and **C60-3PEFe** representative molecules studied in this work in CH_2Cl_2, 0.1 M of Bu_4NPF_6 as electrolyte, at scan rate of 50 mV/s and using a GCE as working electrode.

In contrast, the decrease in the potential with respect to the elongation of the conjugated backbone suggests that there is stabilization of the oxidized species as the conjugated chain is enlarged, as observed for ferrocenyl-phenylenevinylene oligomers [18]. This anodic shift is particularly significant when going from the oligomers to the oligo(fulleropyrrolidines). In general terms, we observed that the C60-pyrrolidine generates an increase of the oxidation potential of the wave assigned to the ferrocene, suggesting that C60 is a stronger electron-accepting group than benzoates, as can be seen from the values in Table 1. It is well known in cyclic voltammetry that the wave potential gives a direct indication of the degree of the electron density transfer, which in this case, is from the ferrocene to the acceptor group; here, the ferrocene gives a higher electron density and will be more difficult to be oxidized, generating a shift to higher potentials. Regarding the cathodic region, we observe only one reduction wave for ferrocene molecules or two reduction waves for the triazene molecules. In general, we assume that the interaction of ferrocene with the electron-accepting groups is strong for the whole series, likely, via dynamic electron transfer that could explain why the distance between the first redox waves is too large with respect to that of the free ferrocene. However, this potential wave is also very wide; we infer that this is because the wave mixes with the signal of each individual reduction group, which are certainly in the whole system being affected by the length and type of the π-bridge and of the electron-accepting type group. In this respect, we observed a similar trend to that of the oxidation potential wave, but in the inverse sense. Thus, the shortest oligomer **HO-1PEFe** exhibits a reduction potential wave (E_{red}) of -1.390 V, which decreases by increasing the conjugation to -1.271 V for **HO-2PEFe** and to -1.025 V for **HO-3PEFe**. In addition, the strength of the electron acceptor group makes these values decrease even more in the order C60-pyrrolidines < benzoates. Based on these results, we can deduce that the character of the HOMO in the series is defined by the ferrocenyl and PE moiety, whereas the character of the LUMO is mainly determined by the electron-accepting group, i.e., C60-fulleropyrrolidine. This was further confirmed by the theoretical simulation of the HOMO and LUMO. Figure 3 reports the frontier orbitals for **C60-2PEN3** and **C60-1PEFe** as representative molecules. It can be observed that the electron density is mainly concentrated in the spatial region of the π-bridge up to triazene or

ferrocene in the HOMOs, while it is localized on the N-methyfulleropyrrolidine in the LUMOs, suggesting strong electronic coupling between the ferrocene or triazene and C60-pyrrolidine. The calculated energies are in good agreement with the experimental values obtained by cyclic voltammetry. For **C60-2PEN3**, HOMOth= -5.85 eV vs. HOMOexp= -5.96 eV and LUMOth= -3.52 eV vs LUMOexp= -3.93 eV. For **C60-1PEFe**, HOMOth= -5.61 eV vs HOMOexp= -5.66 eV and LUMOth= -3.54 eV vs LUMOexp= -3.58 eV.

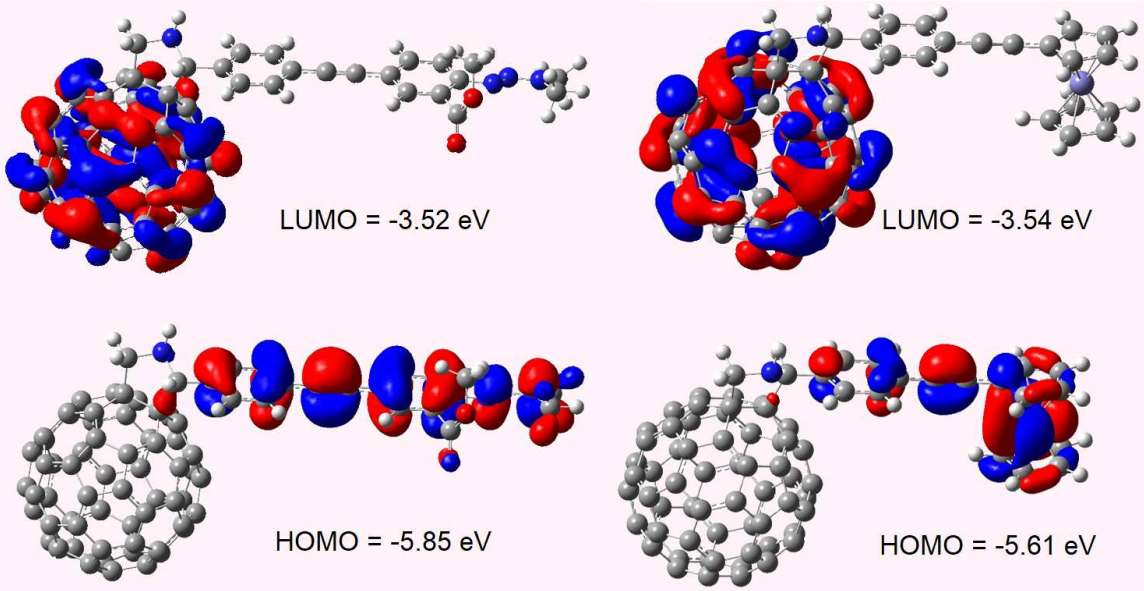

Figure 3. Frontier molecular orbitals; spatial distribution for the HOMO→LUMO energy levels for: Left **C60-2PEN$_3$** and right **C60-1PEFe**, obtained at the B3LYP level with the 6-311+G** and the mixed 6-311+G**(C,N,O,H)/m6-31G*(Fe) basis sets, respectively. The surfaces are calculated at the isovalue of 130 e·nm^{-3} (0.02au).

2.3 Photophysical properties

2.2.1 Triazene terminated dyads

Figure 4 presents the absorption spectra of the **C60-nPEN$_3$** derivatives in CH_2Cl_2 and Table 2 resume all the determined photophysical parameters. The UV-Vis spectra of N-methylfulleropyrrolidyne (**MFP**) and the **HO-nPEN$_3$** oligomers are also included for sake of discussion. The spectrum of **MFP** is similar to that in toluene, previously reported [19]. It presents strong absorptions in the UV at 255 and 327 nm, which for C60 in n-

hexanes have been ascribed to the electronic transitions from the ground state to the 6^1T_{1u} and 3^1T_{1u} excited states, respectively [20]. In the visible region (insert, Figure 4), **MFP** shows a broad absorption with sharp peaks at 430 nm and 702 nm that were assigned to the lowest allowed and the lowest singlet transitions in similar fulleropyrrolidines [9c]. The benzoatheethynylene oligomers show a main absorption peak at 350 nm and 372 nm for **HO-2PEN$_3$** and **HO-3PEN$_3$**, respectively, with increasing absorption coefficient when passing from the dimer to the trimer, in agreement with the extension of the conjugated chain and thus the larger number of chromophores.

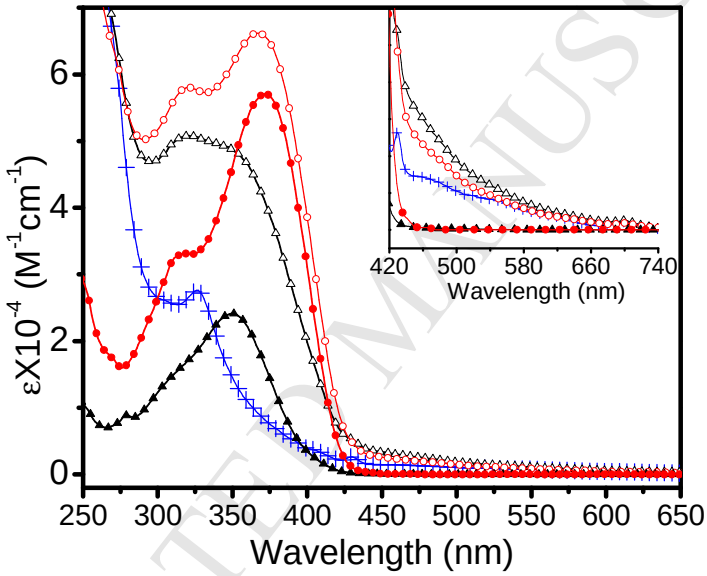

Figure 4. Absorption spectra of **HO-2PEN$_3$** (black filled triangles), **MFP** (blue crosses), **HO-3PEN$_3$** (red filled circles), **C60-2PEN$_3$** (white filled triangles) and **C60-3PEN$_3$** (white filled circles) in CH_2Cl_2. The inset shows the spectra in the 420-740 nm range

A shoulder can be clearly observed at 320 nm for **HO-3PEN$_3$**, while it is just a slight deflexion for **HO-2PEN$_3$**. The fluorescence spectra are identical if the excitation wavelength is on the main peak or the shoulder and present a strong peak at 406 nm for **HO-2PEN$_3$** and 416 for **HO-3PEN$_3$** (Figure 5a). The emission spectrum of the latter molecule is more resolved than that of **HO-2PEN$_3$** exhibiting excitonic features. The fluorescence quantum yield is low because of the quenching effect of the triazene. The excitation spectrum of both molecules (Figure 5b) presents a peak at around 300 nm and a red shifted peak centred at 352 nm for **HO-2PEN$_3$** and 381 nm for **HO-3PEN$_3$,**

which does not change by choosing as the emission wavelength, either the main fluorescence peak or its shoulder at 438 nm. A first comparison with the absorption spectrum suggests that a good match exists for only the lower energy peak. However, after deconvolution of the UV-Vis spectra (Figure 5b for HO-2PEN3 as example), it appears a better match between the absorption and excitation spectra for both peaks.

Table 2. Photophysical properties of **HO-nPEN$_3$** oligomer models and of **C60-nPEN$_3$** dyads in CH_2Cl_2.

Molecule	λ_{abs} (nm)[a]	ε*10^{-4} ($M^{-1}cm^{-1}$)[b]	λ_{emis} (nm)	Φ (%)	Q
HO-2PEN$_3$	**350**	2.4	395	1.10	
HO-3PEN$_3$	320 (sh), **372**	5.7	416	0.20	
C60-2PEN$_3$	**320**, 430, 699	5.1	371	0.16	6.9
C60-3PEN$_3$	320, **367**, 700	6.6	373	0.03	6.7

[a]maximum wavelength (bold and underlined character), [b]at the maximum wavelength

The fact that the fluorescence spectra do not change with excitation wavelength and that the excitation well match the absorption spectra suggest that there is only one emitting species.

The UV-Vis spectra of the C60 derivatives, composed by the absorptions of the corresponding benzoatheethynylenes and **MFP** do not correspond to the sum of the individual spectra, Fig 11S. Similar observations were made by different authors on other C60 derivatives of conjugated oligomers ascribing this behaviour to electronic perturbation between the individual chromophores in the ground state [12d,13d,21]. This effect is more marked for the less conjugated system (**C60-2PEN$_3$**).

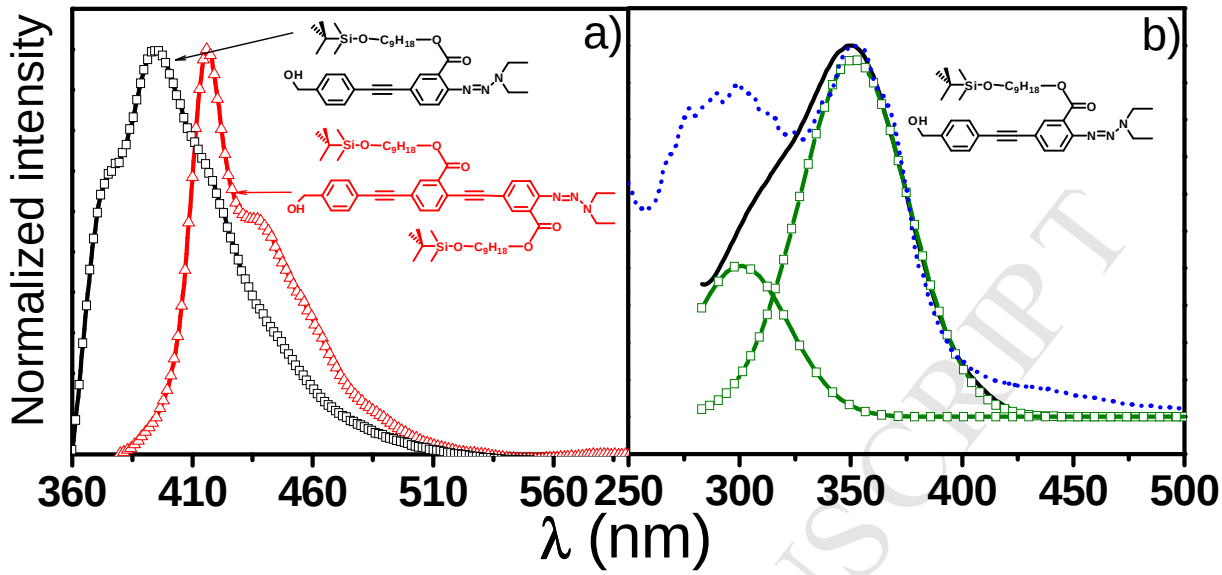

Figure 5. a) Fluorescence spectra of **HO-2PEN$_3$** (black squares) and **HO-3PEN$_3$** (red triangles) in CH_2Cl_2. b) Excitation spectrum (blue dotted line), absorption spectrum (black solid line) of **HO-2PEN$_3$** in CH_2Cl_2 and its corresponding deconvolution absorption bands (green squares).

The maximum wavelength red shifts from **C60-2PEN$_3$** to **C60-3PEN$_3$** due to the increase of the central conjugated length moiety, but blue shifts with respect to the corresponding benzoatheethynylene **HO-nPEN$_3$** precursors, which is in agreement with the electron withdrawing effect of fullerene. The fluorescence spectra of both fullerene derivatives, Fig 13S, are very similar and exhibit excitonic features. The maximum presents a very low bathochromic shift with the increase in the phenylenethynylene segment and a hypsochromic shift with respect to the oligomer precursors. The fullerene emission was not detected, probably because i) of the restricted detection limit of our equipment, ii) it overlaps with the replica at twice the wavelength of the benzoatheethynylene emission, and iii) it was not possible to selectively excite the fullerene moiety. In fact, the UV-bands overlap with the BzE absorptions and the visible absorption bands present a very low absorption coefficient. Attempts to adjust the optical density at 0.1 for the fullerene absorption at 430 nm or 702 nm failed, as the molecules tend to agglomerate at higher concentration. The BzE fluorescence quantum yield, however, decreases after the **MFP** functionalization, suggesting a possible photoinduced energy transfer, even if Förster

energy transfer cannot be discarded as the emission and absorption spectra overlap (see energy considerations *vide infra*).

2.2.1 C60-nPEFe triads

The photophysical properties of the fullerene ferrocene triads (**C60-nPEFe**) in CH_2Cl_2 are reported in Table 3 together with those of the corresponding BzE oligomers (**HO-nPEFe)**. The absorption spectra of both families (benzoatheethynylene and C_{60} derivatives) in CH_2Cl_2 are shown in Figure 6.

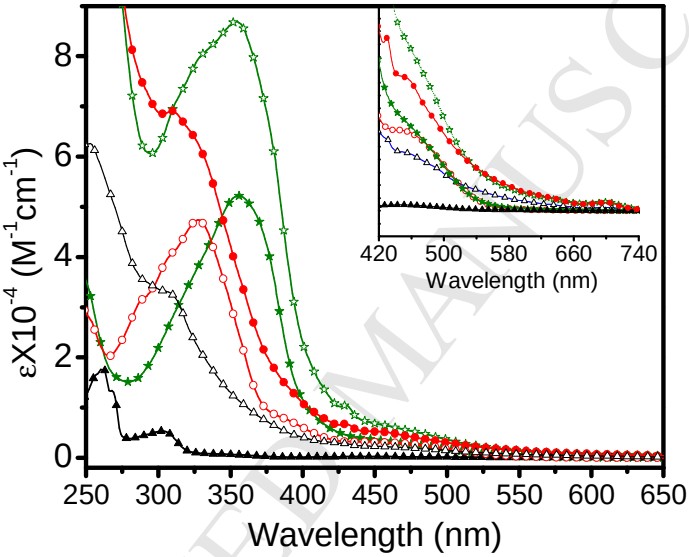

Figure 6. Absorption spectra of **HO-1PEFe** (black filled triangles), **HO-2PEFe** (white filled circles), **HO-3PEFe** (green filled stars), **C60-1PEFe** (white filled triangles), **C60-2PEFe** (red filled circles) and **C60-3PEFe** (white filled stars) in CH_2Cl_2. The inset shows the spectra in the 420-740 nm range.

Both, the ferrocene oligomers and C60 derivatives present a main absorption in the UV due to the π–π* electronic transition of the phenyleethynylene moiety and that shifts in the series according with the increase in the conjugation, but blue shifts from the oligomers to the C60 derivatives due to the electron withdrawing effect of fullerene (see Table 3).

Table 3. Photophysical properties of **HO-nPEFe** oligomer models and of **C60-nPEFe** triads in CH_2Cl_2.

Molecule	λ_{abs} (nm)[a]	$\varepsilon*10^{-4}$ ($M^{-1}cm^{-1}$)[b]	λ_{emis} (nm)	Φ (%)	Q
HO-1PEFe	**303**	0.53	333	1.20	
HO-2PEFe	**328**	4.74	376	10.40	
HO-3PEFe	**356**	5.22	397	15.00	
C60-1PEFe	**304**, 430, 455, 703	3.32	337	0.30	4.0
C60-2PEFe	310, 430, 453, 703	6.91	373	0.60	17.3
C60-3PEFe	**355**, 430, 460, 701	8.69	391	0.06	250.0

[a]maximum wavelength (bold and underlined character), [b]at the maximum wavelength

The spectra of ferrocene and N methylfulleropyridine are reported in Fig 12S together with the sum spectra for each compound. From these figures, it can be observed that the absorption behavior of the ferrocene fullerene triads is similar to that previously discussed for the triazene series, where the absorptions of the individual conforming chromophores, i.e., phenyleneethynylene, ferrocene and MFP, can be visualized, but the spectra do not match the sum of their components.

In the visible, an absorption ranging from 440 to 700 (insert Figure 6) is also observed for the oligomers and is assigned to ferrocene transitions [22]. Concerning the fullerene derivatives, the C60 transition at 430 nm overlaps, giving a neat peak at this wavelength, in addition the fullerene electronic transitions at 255 and 704 nm are also present. From the absorption coefficient of **C60-3PEFe** (Figure 6) and **MFP** (Figure 4), we can deduce an increase of the optical density at 255 nm of 64%, which is a large antenna effect of the oligomer.

In fluorescence, the maximum red shifts along the series, as observed in the absorption spectra, Table 3. Figure 7 shows the excitation, absorption and emission spectra for **C60-3PEFe** and its precursor **HO-3PEFe** as examples. The emission spectra present excitonic features, where the maximum blue shifts for the fullerene derivatives are in agreement with the electron withdrawing effect of this group. The excitation spectra

match well the PE absorption band at around 350 nm. The ferrocene and fullerene (for **C60-3PEFe**) peaks are not observed as these chromophores do not participate in the emission. It is worth mentioning that selective excitation of C60 was not possible due to the overlapping of its absorption with that of the BzE segment. In addition, no fluorescence assignable to fullerene could be detected as in the previous series. However, also in this case, the fluorescence quantum yield strongly decreases with a fluorescence quenching (Q) up to 250 (Table 3), likely indicative of a photoinduced electron transfer process, such as has been reported in other works for similar compounds [9,23,24]. However, energy transfer cannot be discarded as spectral overlap also occurs for this series.

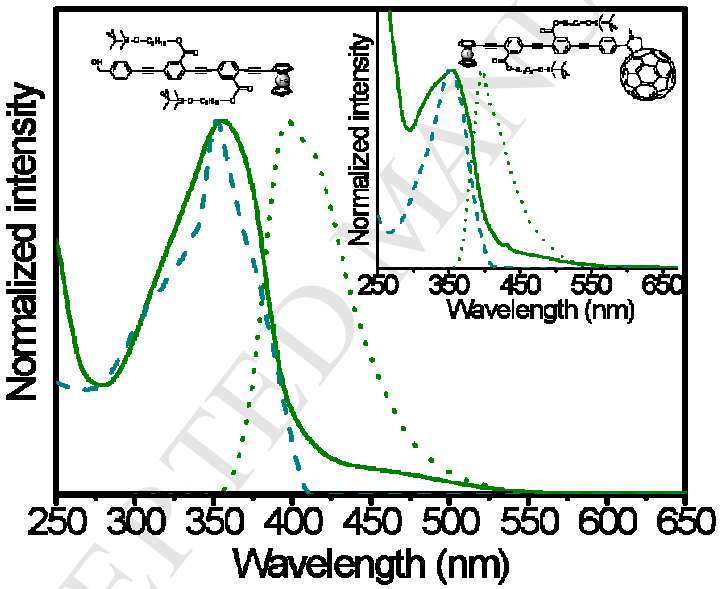

Figure 7. Absorption (solid line), excitation (dashed line) and fluorescence (dotted line) of **HO-3PEFe** and **C60-3PEFe** (inserted figure) in CH_2Cl_2.

2.3. Energy considerations

In order to provide more insight about the fluorescence quenching, energy considerations were realized for **C60-3PEN3** and **C60-3PEFc** as examples of the two series, Table 4.

Table 4. Photoinduced electron transfer parameters and calculated free energy ΔG of C60 dyads and triads in CH_2Cl_2.

Molecule	R_{CC} (Å)	r^+ (Å)	$E_{00,BzE}$ (eV)	ΔG_{BzE} (eV)	G_{CS} (eV)	$\Delta G_{C60\text{-pyrolidine}}$ (eV)	λ	k_r (ns^{-1})	k_{nr} (ns^{-1})	k_{ET} (ns^{-1})
C60-3PEN$_3$	13.9	5.48	3.05	-1.52	1.53	-0.19	0.90	0.04	1.51	5.9
C60-3PEFe	17.8	9.28	3.24	-1.90	1.34	-0.38	0.78	0.05	8.32	498.0

The values of the first excited state of the benzoateethynylene unit (BzE) ($E_{00,BzE}$) was obtained from the interception between the normalized absorption and fluorescence spectrum. The energy of the charged state G_{CS} was calculated by the Weller equation. Based on these energy levels, the possible intramolecular photoinduced processes for these two molecules in CH_2Cl_2 are depicted in Figure 8.

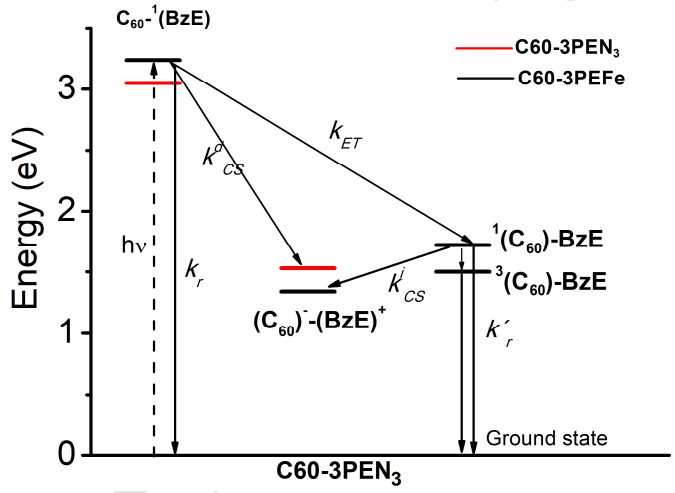

Figure 8. Energy diagram depicting the photoinduced intramolecular process for **C60-3PEN$_3$** and **C60-3PEFe** in CH_2Cl_2.

The direct excitation of the benzoateethynylene (BzE) unit yields to the first excited state C_{60}-^{1}(BE), from which the fluorescence can occur with a radiative constant k_r (=ϕ/τ, Table 4, Fig 14S). The fluorescence quenching is indicative of non radiative competitive processes: energy or photoinduced charge transfer. Direct photoinduced charge transfer processes upon excitation of both BzE and C60-pyrrolidine are exergonic (ΔG<0) because the charge state is at lower energy than both C60-^{1}(BzE) (first excited state of the BE unit) and ^{1}(C60)-BzE (first excited state of C60-pyrrolidine). By calculating the reorganization energy (λ), it was found that direct charge transfer

process from the BzE unit always falls in the inverted Marcus [25] region ($\lambda<-\Delta G_{BzE}$) i.e. it will be followed by charge recombination. Direct charge transfer from the C60-pyrrolidine to BzE unit presents $\lambda>-\Delta G_{C60\text{-}pyrrolidine}$, i.e., after excitation of the fullerene moiety, charge separation should occur. Direct excitation of the fullerene moiety, however, was not experimentally attained as previously mentioned so we cannot confirm if this process is responsible of the fluorescence quenching. Upon excitation of the BE unit, energy transfer from C60-^{1}(BzE) to ^{1}(C_{60})-BzE is also energetically possible, which could follow with fluorescence or phosphorescence (through intersystem crossing) emission of C_{60} and/or to charge transfer. As previously mentioned, emission of C60 was no detected even upon excitation of the BzE unit, so we infer that the fluorescence quenching is mainly due to indirect photoinduced charge transfer: upon excitation of the BzE unit, first energy transfer occurs from BzE to C60-pyrrolidine to BzE reaching the first excited state ^{1}(C60)-BzE. Then, photoinduced charge transfer follows getting the charge state, as found for C60-OPV dyads upon excitation of the OPV unit [9a]. The energy transfer constant $k_{ET}=(Q-1)/\tau_{BE}$ (Table 4) could be obtained from the fluorescence quenching of the BzE unit Q and the fluorescence lifetime of the BzE precursor, τ_{BzE} (0.97 ns and 0.50 ns for **HO-3PEN$_3$** and **HO-3PEFe)**, respectively. This gives a value of two orders larger for the ferrocene compound with respect to the triazene derivative revealing a more efficient energy transfer, as first deactivation process, for this triad.

2.6 Photovoltaic properties

From all of the series, just **C60-3PEN$_3$** and **C60-3PEFe** gave moderate optical quality films on ITO, thus photovoltaic properties were tested: 1) intrinsically; as molecular cables and 2) mixed with the P3HT electron donor material by substituting the PC61BM as electron attractor material. The active layer was sandwiched between PEDOT:PSS and aluminum or Field's Metal electrodes, without significant differences from one to the other cathode as has been reported [26]. Since, devices were tested at ambient conditions, a P3HT:PC61BM (1:1 wt. %) device was built as a reference yielding a $\eta_{AM1.5}$ = 1.77 %, while in the literature under the same conditions a $\eta_{AM1.5}$ = 1.54 % for

P3HT:PCBM-C61 (1:3 wt. %) is reported, Fig 15S [27]. Table 5 summarizes all of the determined photovoltaic parameters.

As active materials in molecular cables cells both oligo(fulleropyrrolidines) **C60-3PEN$_3$** and **C60-3PEFe** gave very low power conversion efficiencies (order of 10^{-7}), which increased by two orders of magnitude (to 10^{-5}) by adding an interfacial cathode layer of PFN (< 5 nm), meaning that there is a better electron recollection to the cathode, but still with low values.

Table 5. Resume of several tested active layer compositions and the determined photovoltaic parameters for each material combination.

Solar cell composition	*Jsc (mA/cm^2)*	*Voc (mV)*	*FF*	*η (%)*
P3HT:PCBM-C60 (1:1)	6.37	400	0.69	1.77
C60-3PEN$_3$	3.13 X 10^{-5}	48	0.001	4.3 X 10^{-7}
C60-3PEFe	2.5 X 10^{-5}	130	0.078	6.8 X 10^{-7}
C60-3PEN$_3$/PFN	1.0 X 10^{-4}	560	0.260	1.7 X 10^{-5}
C60-3PEFe/PFN	2.0 X 10^{-4}	428	0.260	2.5 X 10^{-5}
P3HT: C60-3PEFe (1:2)	0.002	604	0.210	2.3 X 10^{-3}

According to the energy diagram, the $\Delta LUMO_{P3HT\text{-}C60\text{-}3PEFe}$ = 0.32 eV suggests that charge transfer to P3HT is possible, so, after having evaluated different processing conditions, which are reported in the legend of Figure 9, the best obtained efficiency for the heterojunction configuration was of $\eta_{AM1.5}$ = 0.002 %; i.e. a 4 orders of magnitude higher than that as molecular cable. The Voc has a good value (604 mV), while the current density 0.023 mA/cm^2 is still poor and in general, the photovoltaic values are lower compared with that of P3HT:PC61BM cell. In this respect, we can identify at least two factors that limit the intrinsic efficiency of the **C60-3PEFe** based devices in both architectures. First, considering Figure 9b, its absorption spectrum in film of c.a. 133 nm presents the HOMO-LUMO electronic transition at 364 nm that is out of the maximum of the solar irradiance spectrum, then a drastic shut down of the absorption coefficient (ε_t) is observed after 364 nm, meaning low solar light absorption of the film in the visible range. This is more evident when the photonic recollection (I_h) spectrum of the **C60-**

3PEFe is compared with the solar irradiance. The maxima photonic recollection I_h ~4.53x10^{6}Wm^{-2}nm^{-1} is obtained at 400 nm and afterwards, it dramatically decreases to the point that at 500 nm the I_h is less than half. The film absorbs 78.4 Wm^{-2} of the 900 Wm^{-2} of solar irradiance energy (at AM1.5), representing only the 8.7 % of absorbed photons. Secondly, low fill factors (FF) are found: 0.078 for **C60-3PEFe** and 0.210 for the P3HT:**C60-3PEFe** devices, Table 5, compared to 0.69 for the P3HT:PCBM device, Fig 15S, ESI. This is likely a consequence of both recombination of charge carriers, in agreement with the photophysical results and to the poorly ordered morphology of the active layers. AFM analysis reveals in fact that **P3HT:C60-3PEFe** device morphology is composed of agglomerates of different size coexisting with a more planar morphology, but an amplification of one of these zones reveals deep valleys of c.a. 500 nm in diameter and of c.a. 25 nm of Z amplitude, Figure 9c-d, evidencing the morphological discontinuity in the film. In contrast, the AFM image of the **P3HT:C60-3PEFe** device, Fig 15 Sc, shows a more homogeneous film.

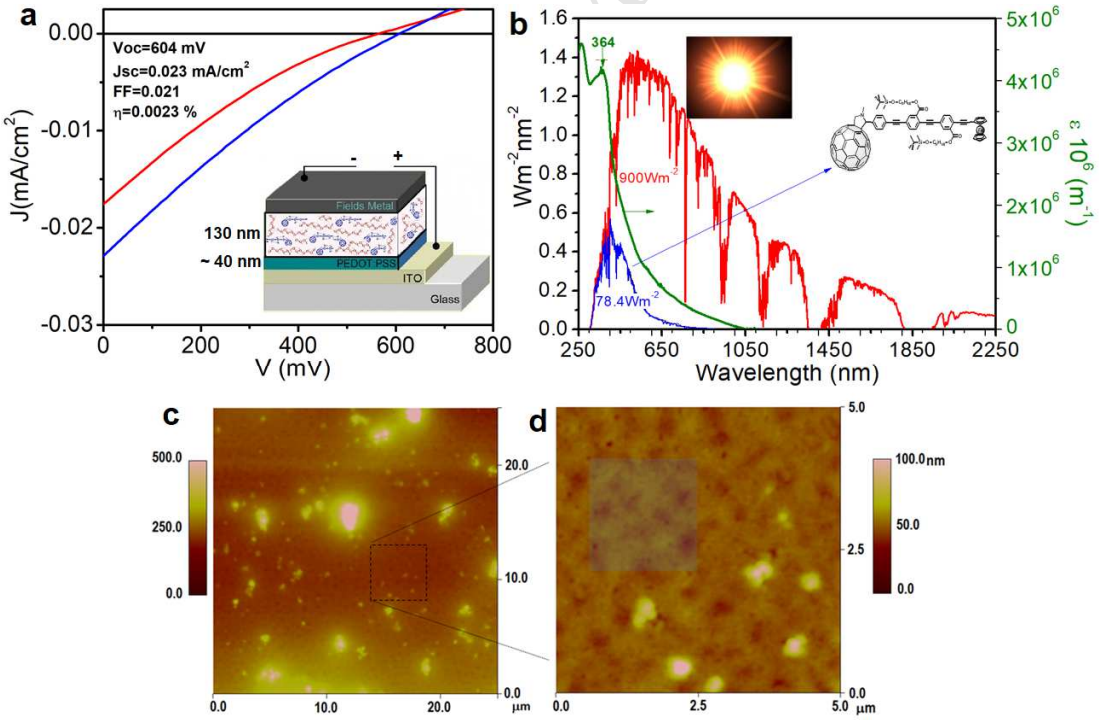

Figure 9. (a) Structure of the P3HT:C60-3PEFe (1:1 w %) solar cell, with thicknesses of 40 nm for the PEDOT:PSS layer and of 130 nm for the active layer. Both layers underwent annealing at 80 °C for 30 min after their individual deposition, Fields Metal as

top contact. (b) Spectra of: solar irradiance (red), photonic recollection (blue) and absorption coefficient in thin film of **C60-3PEFe**. (c) Tapping AFM mode image of the ITO/PEDOT:PSS/P3HT:**C60-3PEFe** film and (d) is an amplification zone.

The aggregates and the inhomogeneity of the film are responsible for the exciton diffusion-dissociation in the films not being carried out and that efficiencies of device constructed with both fulleropyrrolidines are extremely low. In addition, it is likely that the molecules do not have an adequate balance of electron donor-acceptor character, as the benzoate is a poor electron acceptor group. This hypothesis could be corroborated when we compared our results with those found by Nierengarten et al. [28] on fullerene-oligo(phenyleneethynylene)s bearing bis(octyloxy) as side chains (which are electron donor groups). The authors report efficiencies in the order of $\eta = x10^{-2}$ % for devices in configuration ITO/PEDOT:PSS/Oligo(PPE-fulleropyrrolidine)/Al. In general, we conclude that these particular series of oligo(benzoateethynylene)s-either ferrocene or triazene terminated macromolecules are not adequate for photovoltaic devices. ~~and however are very thermal stable up to 150 °C, Fig 16S.~~

3. Conclusions

We succeeded in the synthesis of a novel series of oligomers as precursors and models of the oligo(fulleropyrrolidines) with increasing length, and, connecting the ferrocene or triazene as electron-donor group and C60-pyrrolidine as electron-accepting group in a configuration D→π→A; the benzoates that serve as solubilizing side chains, have a weak electron-accepting character. All of the ferrocene compounds with and without fulleropyrrolidines, *in solution*, oxidize time dependently, becoming insoluble likely due to the fact that ferrocene not only is a good electron donor but an excellent light trapping group; phenomenon that was corroborated by cyclic voltammetry, where either in the oxidation or in the reduction cycle an insoluble precipitate was formed. The oligomers and oligo(fulleropyrrolidines) bearing ferrocene revealed an electrochemically reversible one-electron oxidation wave, which shifted anodically with respect to free ferrocene, but cathodically depending on the length of the π-bridge and of the strength of the electron-accepting group in the order C60-pyrrolidines > benzoates. In contrast, in

the reduction cycle, only one wide wave was observed which shifted anodicaly as a function of both the length of the π-bridge and of the strength of the electron-accepting group in the order C60-pyrrolidines < benzoates. These results suggest the existence of electron transfer between the iron centre of the ferrocene to the electron-accepting groups through the π-bridge. The photophysical study showed a strong fluorescence quenching and higher non-radiative constants of the benzoatheethynylene moiety after functionalization with triazene and even stronger, in the case of ferrocene. The energy considerations suggest that intramolecular photoinduced charge transfer is possible, upon direct excitation of the fullerene moiety or indirectly, after energy transfer from the BzE unit to C60-pyrrolidines, in case of excitation of the conjugated moiety. Nevertheless, as the absorption range of the oligomers is out of the maximum solar irradiance and due to inhomogeneous organization in films, photovoltaic devices present low efficiencies.

4. Experimental Section

4.1 Instruments. ^{1}H (300 MHz), DQF-COSY, DEPT-135, APT, ^{13}C (75.4 MHz) NMR spectra were obtained at room temperature with a Jeol Eclipse spectrometer using $CDCl_3$ as solvent and internal reference. The photophysical characterization was carried out in Aldrich spectroscopic grade CH_2Cl_2. UV-Vis and fluorescence spectra were recorded on an Agilent 8453 spectrophotometer and a Perkin Elmer LS50B spectrofluorimeter, respectively. Fluorescence quantum yield (ϕ) was obtained according to literature method [29] with quinine sulphate (0.1M in H_2SO_4) as standard. Three different solutions with optical density at the excitation wavelength < 0.1 were analyzed at 25.0±0.3 °C by using a circulating water bath and the values were averaged. The excitation wavelength was 10 nm below the absorption maximum. Lifetimes were obtained by TCSPC (time-correlated single photon counting) with a Tempro Horiba instrument with a 285 nm nanoLED. A 0.01% suspension of Ludox AS40 (Aldrich) in ultrapure water was used for the prompt signal. Calibration of the equipment was realized with a POPOP [1,4-Bis(4-methyl-5-fenil-2-oxazolyl)benzene] methanol solution (optical density < 0.1 and lifetime of 0.93ns [30]. Data were fit using DAS6 software available with the equipment. The electrochemical properties of all of the compounds were investigated via cyclic voltammetry in a Stand cell from Basi, coupled

to an ACM Gill AC potentiostat/galvanostat. The system consisted of a conventional three-electrode cell: glassy carbon as a working electrode (polished with alumina and diamond powder after each run), Pt wire as the counter electrode, Ag/AgCl as reference electrode (viability of -35 ± 20 mV against the Calomel electrode). Voltammetry measurements were performed at room temperature in CH_2Cl_2 containing Bu_4NPF_6 (0.1M) as the supporting electrolyte. Prior to recording the voltammograms, all solutions (~0.5 mmol) were deoxygenated by bubbling nitrogen for at least 15 min. The experiments were carried out under a nitrogen atmosphere at a scanning rate of 50-100 mV/s for a complete cycle between -3.0 and +3.0 V and in separated windows. The molecular orbital energies HOMO and LUMO were calculated according to the empirical relationship [27]: $E^{HOMO[LUMO]}$= -exp($E_{(Ox[red]vs.\ Ag/AgCl)}$)-4.80. Solar cells were fabricated with the configuration: ITO/PEDOT:PSS/active layer/Al or Field´s metal. The ITO slides (15-30 ohms) were cleaned in a Branson ultrasonic bath with different solvents: 1) methylene chloride (10 min); 2) hexane (10 min) and 3) methanol (two cycles of 20 and 40 min, respectively). PEDOT:PSS and the active layers were deposited by spin coating with a WS-400-6NPP-LITE spin coater from Laurel Technologies. Commercial PEDOT:PSS suspension was first filtered in a syringe 0.45 micro filter and then spin coated on the ITO slides at 5000 rpm for 25 s and at 2500 rpm for 1min. The PEDOT:PSS layer (approximately 20 nm) was dried in an oven at 80 °C for 30 min before the following deposition step. Active layers consisted of: i) **P3HT:PCBM-C60** as comparative term. In this case, a 1 wt/wt chlorobenzene solution of P3HT:PCBM-C60 was prepared and kept 12h at 60 °C under magnetic stirring. The mixture was maintained 1h at room temperature under magnetic stirring and then spun at 800 rpm on the PEDOT:PSS layer to obtain a layer of approximately 100 nm. ii) As molecular cable, **C60-3PEFe** was stirred in chlorobenzene and for 12h at 50°C. The mixture was maintained 1h at room temperature under magnetic stirring and then spun at 1500 rpm on the PEDOT:PSS layer to obtain a layer of approximately 100 nm. iii) **P3HT:C60-3PEFe:** 1 wt/wt chlorobenzene solution of P3HT:C60-3PEFe was dissolved in chlorobenzene and kept at 50 °C under stirring. The mixture was maintained 1h at room temperature under magnetic stirring and then spun at 1200 rpm to obtain a layer of c.a. 130 nm. Then, the active layer was annealed at 150 °C for 30 min. Al or Field's metal

(FM) as cathode were deposited by vacuum evaporation (Al) or at 85 °C by using a heating plate (FM). The I-V curves were obtained with a Keithley 2420 source meter by illuminating the devices from the ITO side with a 100 mW/cm^2 white light from a Solar Light Co. Model XPS 400 solar simulator with a Xenon lamp and AM1.5 filter. All cells were prepared and measured under ambient conditions. The film thickness was determined using a perfilometer Veeco Dektak 6M Stylus with a 12.5 μm radius tip at a speed rate of 50 μm/s and an applied force of 2 milligrams. Morphological characterization of the active layers by AFM was performed on a Nanoscope III DimensionTM 3100 from Digital Instruments with a Pt-coated Si tip (15 nm nominal radius, model OSCM-PT from Bruker) in tapping mode at a scanning rate (256 lines) of 0.2 Hz.

4.2. ***Synthesis.*** Experimental procedures, chemical and physicochemical characterization of each compound are given in the electronic supplementary information section.

4.3. ***Theoretical calculations*****.** Theoretical calculations were carried out using the Gaussian 09 software using B3LYP functional with the 6-311+G** basis set for C,N,H,O and m6-31G* one for Fe. The latter provides a more appropriate description of the first-row transition metals.

Acknowledgments

We wish to acknowledge the Mexican National Council for Science and Technology for the financial support through the projects CB-2015: 256716 and 256709, National Laboratory of Graphene. Authors also thank to Guadalupe Méndez and Alfonso Mercado for their technical help.

Electronic Supplementary Information (ESI) available: experimental procedures, ^{1}H, ^{13}C, DQF COSY, HETCOR NMR spectra, excitation and fluorescence spectra, fluorescence time decay profiles of selected oligomers and a P3HT:PC60BM solar cell device are found at htpp//...

References

[1] N. S. Sariciftci, L. Smilowitz, A. J. Heeger, F. Wudl, Science 258 (1992) 1474-1476.

[2] M. Li, K. Gao, X. Wan, Q. Zhang, B. Kan, R. Xia, F. Liu, X. Yang, H. Feng, W. Ni, Y. Wang, J. Peng, H. Zhang, Z. Liang, H.-L. Yip, X. Peng, Y. Cao, Y. Chen, Nat. Photonics 11 (2017) 85–90.

[3] W.-Y. Wong, X.-Z. Wang, Z. He, A.B. Djurišić, C.-T. Yip, K.-Y. Cheung, H. Wang, C.S.-K. Mak, W.-K. Chan, Nat. Mater. 6 (2007) 521.

[4] A.Z. Weller, Phys. Chem. Neue Folge 133 (1982) 93-98.

[5] A. Manzano-Ramírez, E.J. López-Naranjo, W. Soboyejo, Y. Meas-Vong, B. *J.* Vilquin, J. Nanomater. 2015 (2015) 1-15.

[6] S. Cataldo, P. Salice, E. Menna, B. Pignataro, Energy Environ. Sci. 5 (2012) 5919-5940

[7] C. Li, H. Wonneberger, Adv. Mater*.* 24 (2012) 613–636.

[8] T. Liu, A. Troisi, Adv. Mater. 25 (2013) 1038–1041.

[9] (a) E. Peeters, P.A. van Hal, J. Knol, C.J. Brabec, N.S. Sariciftci, J.C. Hummelen, R.A.J. Janssen, J. Phys. Chem. B 104 (2000) 10174-10190.

(b) R. Gómez, J.L. Segura, Tetrahedron 65 (2009) 540-546.

(c) J.-F. Eckert, J.-F. Nicoud, J.-F. Nierengarten, S.-G. Liu, L. Echegoyen, F. Barigelletti, N. Armaroli, L. Ouali, V. Krasnikov, G. Hadziioannou, J. Am. Chem. Soc*.* 122 (2000) 7467-7479.

(d) D.vZhu, Y. Li, S. Wang, Z. Shi, C. Du, S. Xiao, H. Fang, Y. Zhou, Synth. Met*.* 133-134 (2003) 679-683.

[10] (a) A. Marcos Ramos, S.C.J. Meskers, P.A. Van Hal, J. Knol, J.C. Hummelen, R.A.J. Janssen, J. Phys. Chem. A 107 (2003) 9269-9283.

(b) J-G. Domínguez-Chávez, E. Cruz-Chávez, I. Moggio, E. Arias-Marín, T. Klimova, I. Lijanova, M. Martínez-García, Fullerenes, Nanotubes, and Carbon Nanostructures 20 (2012) 249–265.

[11] W.-Y. Wong, C.-L. Ho, Acc. Chem. Res. 43 (2010) 1246-1256.

[12] (a) J.L. Segura, R. Gómez, N. Martín, C. Luo, A. Swartz, D.M. Guldi, Chem. Commun. (2001) 707–708.

(b) D.R. Guldi, A. Swartz, C. Luo, R.G ómez, J.L. Segura, N. Martín, J. Am. Chem. Soc. 124 (2002) 10875-10886.

(c) T. Gu, P. Ceroni, G. Marconi, N. Armaroli, J-F. Nierengarten, J. Org. Chem. 66 (2001) 6432-6439.

(d) Accorsi, G.; Armaroli, N.; Eckert, J.-F.; Nierengarten, J.-F. *Tetrahedron Lett.* **2002**, 43, 65–68.

[13] (a) A. Lembo, P. Tagliatesta, D.M. Guldi, M. Wielopolski, M. Nuccetelli, J. Phys. Chem. A 113 (2009) 1779–1793.

(b) M. Wielopolski, C. Atienza, T. Clark, D.M. Guldi, N. Martín, Chem. Eur. J. 14 (2008) 6379–6390.

(c) N. Armaroli, G. Accorsi, Y. Rio, P. Ceroni, V. Vicinelli, R. Welter, T. Gu, M. Saddik, M. Hollerd, J-F. Nierengarten, New J. Chem. 28 (2004) 1627–1637.

(d) J.N. Clifford, T. Gu, J-F. Nierengarten, N. Armaroli, Photochem. Photobiol. Sci. 5 (2006) 1165-1172.

[14] M. Maggini, G. Scorrano, M. Prato, J. Am. Chem. Soc. 115 (1993) 9798-9799.

[15] S.-G. Liu, L. Shu, J. Rivera, H. Liu, J. –M. Raimundo, J. Roncali, A. Gorgues, L. Echegoyen, J. Org. Chem. 64 (1999) 4884-4886.

[16] J. Palomero, J.A. Mata, F. González, E. Peris, New. J. Chem. 26 (2002) 291-297.

[17] J.N.Wilson, P.M. Windscheif, U. Evans, M. L. Myrick, U.H.F. Bunz, Macromolecules 35 *(*2002) 8681-8683

[18] J. A. Mata, S. Uriel, R. Llusar, E. Peris, Organometallics 19 (2000) 3797-3802.

[19] M. Prato, M. Maggini, Acc. Chem. Res. 31 (1998) 519-526.

[20] S. Leach, M. Vervloet, A. Després, E. Bréheret, J. P. Hare, T. J. Dennis, H. W. Kroto, R. Taylor, D. R. M. Walton, Chem. Phys. 160 (1992) 451-466.

[21] (a) R. Seshadri, C. N. R. Rao, H. Pal, T. Mukherjee, J. P. Mittal, Chem. Phys. Lett. 205 (1993) 395–398.

(b) M. C. Rath, H. Pal, T. Mukherjee, J. Phys. Chem. A 103 (1999) 4993–5002.

[22] (a) H. Zhao, Y. Zhu, C. Chen, J. Zheng, Carbon 50 (2012), 4894-4902.

(b) P.K. Poddutoori, A.S.D. Sandanayaka, T. Hasobe, O. Ito; A. Van der Est, J. Phys. Chem. B 114 (2010) 14348-14357.

[23] H. Kanato, K. Takimiya, T. Otsubo, Y. Aso, T. Nakamura, Y. Araki, O. Ito, J. Org.

Chem. 69 (2004) 7183-7189.

[24] P.A. Van Hal, J. Knol, B.M.W. Langeveld-Voss, S.C.J. Meskers, J.C. Hummelen, R.A.J. Janssen, Synth. Met. 116 (2001) 123-127.

[25] R. A. Marcus, J. Chem. Phys. 43 (1965) 679-701.

[26] A. Du Pasquier, S. Miller, M. Chhowalla, Sol. Energ. Mat. Sol. Cells 90 (2006) 1828-1839.

[27] M. Al-Ibrahim, H.-K. Roth, M. Schroedner, A. Konkin, U. Zhokhavets, G. Gobsh, P. Scharff, S. Sensfuss, Org. Electron. 6 (2005) 65-77.

[28] T. Gu, D. Tsamouras, C. Melzec, V. Krasnikov, J.-P. Gisselbrecht, M. Gross, G. Hadziioannou, J.-F. Nierengarten, Chem Phys Chem 1 (2002) 124-127.

[29] A.T.R. Williams, S.A. Winfield, J.N. Miller, Analyst 108 (1983) 1067-1071.

[30] S.A. El-Daly, S.A. El-Azim, F.M. Elmekawey, B.Y. Elbaradei, S.A. Shama, A.M. Asiri, Int. J. Photoenergy 2012 (2012) 1-10.